Conjugate Heat Transfer in a Rectangular Channel with Perforated Protrusion and Cross-Flow Effect

N. Smruti Chhanda and Ashok K. Barik*

Department of Mechanical Engineering, College of Engineering and Technology, Bhubaneswar, Odisha, India
*E-mails: smrutichhanda91@gmail.com; *Corresponding: E-mail-ashokbarik.mech@gmail.com*

Abstract: Heat transfer enhancement from a heated surface fitted with solid and perforated protrusions has been studied numerically employing the finite volume method for solving the governing equations for mass, momentum, and energy in a 3-D computational domain. SST k–ω model has also been solved to close the governing equations and to get the turbulent quantities. The duct Reynolds number has been varied in the range of $15,000 \leq \mathrm{Re}_{Dh,Duct} \leq 46,000$, and the nozzle Reynolds number is maintained constant at $\mathrm{Re}_{Dh,Nz} = 5,134$. It has been observed that the heat transfer enhancement is strongly dependent on the jet impingement and the type of surface protrusions fitted to the bottom heated plate. The pumping power has been found to be higher with perforated protrusions than the solid protrusions.

Keywords: Perforated Protrusions, SST k–ω model, Jet Impingement, Heat Transfer Enhancement

I. INTRODUCTION

A hybrid cooling strategy which utilizes the benefits of heat transfer enhancement by forced convection, jet impingement, surface protrusions as well as perforation in the protrusions has been proposed in the present study. Due to the surface constrains imposed by the miniaturized electronic devices, it is required to dissipate more heat from a small area so as to attain a higher operating speed and durability. Thus, the new and innovative designs are the need of hour to cope up with the miniaturization concept. Mudawar [1] and Yeh [2] have carried out a comprehensive study on the different techniques applied to electronics cooling. Geometrical modifications help in augmenting the heat transfer rate from a heated surface. Heat transfer from the hot wall can be enhanced by putting turbulators of various shapes such as transverse ribs [3-4], W- shaped ribs [5], and V-shaped ribs [6]. Heat transfer rate can be further improved by using perforated ribs instead of the solid ribs. The perforation in the ribs breaks the viscous sub-layer near the heated surface resulting in a better mixing of the cold and hot fluids. Therefore, the heat transfer rate with perforated protrusions is higher than that of the solid protrusions. Karwa *et al.* [7] and Karwa and Maheshwari [8] studied the heat transfer enhancement for heated surface attached with full and half perforated baffles. Bhuiya *et al.* [9] studied the heat transfer characteristics of tubes fitted with perforated inserts. The experimental result of Alam *et al.* [10] showed a significant improvement (i.e., 33%)

when solid V-shaped blockages are replaced with perforated V-shaped blockages. Zhou and Feng [11] investigated the heat transfer enhancement by different shapes of surface protrusions such as rectangular, trapezoidal and delta. Moreover, the heat transfer rate can also be improved by using an impinging jet. It has been demonstrated by various researchers [12-15] that a higher heat transfer rate can be achieved with jet impingement method than that of the forced convection method. As far as the authors' knowledge is concerned, the combined effect of jet impingement, surface protrusions with perforations has not drawn much attention of researchers. Thus, in the present investigation, we have employed the hybrid method (i.e., combined effect of jet impingement, forced convection and surface protrusions along with the perforations, drilled in it) to reveal its effect on the heat transfer enhancement from a heated surface.

II. MATHEMATICAL MODELING

In the present numerical investigation, a rectangular duct of size 0.67 m × 0.023 m × 0.03 m has been used as shown in Fig. 1. Air enters the inlet of the rectangular duct at velocity and temperature of u_{in} and T_∞, respectively. Also, air is impinged normal to the main flow by placing a square nozzle on the top surfaces of the duct so that it will form a cross flow to the main duct flow. This will enhance the mixing, and hence, increase the heat transfer rate from the bottom hot surface. Moreover, rectangular protrusions have been provided on the bottom hot surface to further augment the heat transfer rate. The hot surface (of length $X / Dh_{duct} = 5.76$) is maintained at a constant temperature ($T_w = 373K$). An extra length of 10 times the hydraulic diameter of the duct has been considered so as to ensure a fully developed flow in the duct. Similarly, an extra length of 10 times the hydraulic diameter is taken in downstream of the hot surface to reduce the effect of backflow at the exit. The rectangular protrusions are perforated with square cross-section of size 0.004 m × 0.004m.
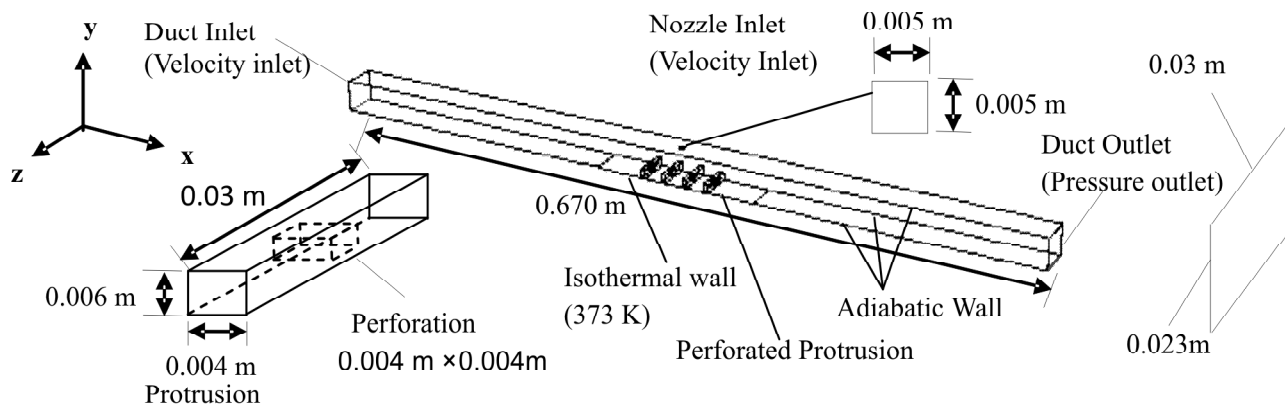

Figure 1: Physical model of the rectangular duct with rectangular protrusions and square perforations along the flow direction

The inlets and outlets of the duct are meshed with triangular cells. The bottom surface except the hot wall is meshed with rectangular cells in order to control the number of cells. Tetrahedral meshes have been adopted to mesh the hot surface along with the protrusions. Therefore, the total computational domain is meshed with a hybrid meshing scheme (i.e., combination of hexahedral and tetrahedral meshes). The hydraulic diameter of the nozzle is 0.005 m. Following assumptions are taken to solve the governing equations:

1. The working fluid (air) is Newtonian and incompressible.

2. Flow is steady, three-dimensional and turbulent.

3. Fluid properties such as thermal conductivity (λ), dynamic viscosity (μ), and specific heat (c_p) are kept constant.

III. MATHEMATICAL FORMULATION

3.1. Governing differential equation

The Reynolds time-averaged equations for mass, momentum, energy in an inertial reference frame are written as follows:

Continuity equation:
$$\frac{\partial \overline{u_i}}{\partial x_i} = 0 \tag{1}$$

Momentum equation:
$$\rho \overline{u_i} \frac{\partial \overline{u_i}}{\partial x_i} = -\frac{\partial \overline{p}}{\partial x_i} + \frac{\partial}{\partial x_j}\left(2\mu \overline{S_{ij}} - \rho \overline{u_i' u_j'}\right) \tag{2}$$

Energy equation:
$$\rho \overline{u_j} \frac{\partial \overline{T}}{\partial x_j} = \frac{\partial}{\partial x_j}\left(\frac{\lambda}{c_p} \frac{\partial \overline{T}}{\partial x_i} - \rho \overline{u_i' T'}\right) \tag{3}$$

The mean stain rate is defined as:
$$\overline{S_{ij}} = \frac{1}{2}\left(\frac{\partial u_i}{\partial x_j} + \frac{\partial u_j}{\partial x_i}\right) \tag{4}$$

Where μ, λ and c_p represent the dynamic viscosity, thermal conductivity and specific heat at constant pressure for the working fluid, respectively. The Reynolds stress ($-\rho \overline{u_i' u_j'}$) and turbulent heat flux ($-\rho \overline{u_i' T'}$) terms are appearing due to the time averaging, and these terms need to be closed by using the appropriate turbulence model. The Reynolds stress can be specified using a linear eddy viscosity model as follows:

$$-\rho \overline{u_i' u_j'} = 2\mu_t \overline{S_{ij}} - \frac{2}{3}\rho k \delta_{ij} \tag{5}$$

Where, k denotes the turbulent kinetic energy and μ_t represents the eddy viscosity, which are to be specified by solving the transport equations for the turbulent kinetic energy (k) and specific dissipation rate using the k–ω turbulence model. Similarly, the turbulent heat flux is defined as

$$-\rho \overline{u_i' T'} = \frac{\mu_t}{Pr_t} \frac{\partial \overline{T}}{\partial x_i} \tag{6a}$$

Here, Pr_t denotes the turbulent Prandtl number. The SST k–ω turbulence model proposed by Mentor [21] is implemented in the present study so as to model the turbulence quantities. The governing equations for the turbulence kinetic energy (k) and specific dissipation of turbulence kinetic energy (ω) are written as follows [18].

$$\frac{\partial}{\partial x_i}(\rho k u_i) = \frac{\partial}{\partial x_j}\left[\left(\mu + \frac{\mu_t}{\sigma_k}\right)\frac{\partial k}{\partial x_j}\right] + \min(P_k, 10\rho\beta^* k\omega) - \rho\beta^* k\omega \tag{6b}$$

$$\frac{\partial}{\partial x_i}(\rho \omega u_i) = \frac{\partial}{\partial x_j}\left[\left(\mu + \frac{\mu_t}{\sigma_k}\right)\frac{\partial \omega}{\partial x_j}\right] + \frac{\alpha\omega}{k}P_k - \rho\beta\omega^2 + 2(1-F_1)\frac{\rho\sigma_{\omega,2}}{\omega}\frac{\partial k}{\partial x_j}\frac{\partial \omega}{\partial x_j} \tag{6c}$$

The eddy viscosity is written as

$$\mu_t = \rho \frac{k}{\omega} \frac{1}{\max\left(\frac{1}{\alpha}, \frac{SF_2}{a_1 \omega}\right)}$$

(6d)

Different model constants used in the SST k–ω turbulence model are given as follows:

$\alpha_\infty^* = 1, \beta_\infty^* = 0.09, \beta_i = 0.072, \sigma_{k,1} = 1.176, \sigma_{\omega,1} = 2, \sigma_{k,2} = 1, \sigma_{\omega,2} = 1.168, R_k = 6, a_1 = 0.31$ and $R_\beta = 8$. The heat transfer coefficient and Nusselt number have been calculated as follows:

$$h = \frac{Q}{A_{tot}(T_w - T_\infty)}$$

(7)

$$A_{tot} = A_{bw} + A_p + A_{perf}$$

Here the total are (A_{tot}) is the sum of bare area of hot wall (A_{bw}), area of protrusions (A_p), area of perforation (A_{perf}).

$$Nu = \frac{hL}{\lambda}$$

(8)

3.2. Boundary condition

The applied boundary conditions for present the computational domain has been shown in Fig. 1.The constant velocity inlet condition has been imposed at the duct and nozzle inlets. The pressure outlet boundary condition is applied to the outlet of the duct since the flow is issued on the ambient condition. The front and back side walls are kept adiabatic. Similarly, the top wall (excluding the nozzle inlet) has been maintained adiabatic. The bottom wall, excluding the heated surface along with the perforated protrusions is adiabatic. A constant temperature boundary condition is applied to the heated surface.

The mathematical descriptions of different boundary conditions are given as follows:

At adiabatic walls: $\quad u = v = w = 0$, and $\dfrac{\partial T}{\partial x} = \dfrac{\partial T}{\partial y} = \dfrac{\partial T}{\partial z} = 0$ (9)

At solid isothermal wall: $\quad u = v = w = 0$ and $T = T_w$ (10)

At duct inlet: $\quad u_p = u_{in}, T = T_\infty$ (11)

At nozzle inlet: $\quad v = -v_{in}, T = T$ (12)

Here u, v and w are the velocity components in the x, y, and z- direction, respectively.

At pressure outlet: $\quad p = p_\infty$ and $T = T_\infty$ (13)

Where, p_∞ and T_∞ are the ambient pressure and temperature, respectively.

IV. NUMERICAL SOLUTION PROCEDURE

Conservation equations for mass, momentum, energy are discretized in a three-dimensional computational domain imposing appropriate boundary conditions. Since the mean flow is turbulent, the SST $k-\omega$ model has been

employed to solve the turbulent kinetic energy (k) as well as its specific dissipation rate (ω) equations. The second order upwind scheme has been used to discretize the advection terms, while central difference scheme is used to discretize the diffusion terms. Since both the discretization schemes are 2nd order accurate, so we decided to use those. The set of algebraic equations resulting from the discretization of the equations is solved iteratively using commercial software ANSYS Fluent 16. SIMPLE algorithm has been used for the pressure velocity coupling, and the pressure is updated at the end of the iteration. The SST k–ω model has been preferred over the other variants of the models since we expect a strong flow recirculation in the computational domain due to the presence of the perforated surface protrusions. Also, the addition of an impinging jet to the main flow imparts further recirculation and mixing in the computational domain.

V. VALIDATION AND NUMERICAL METHODOLOGY

The present numerical scheme has been validated with some of the existing experimental data available in the literature. However, the heat transfer augmentation and thermal management of a mini rectangular channel with surface protrusions and the cross flow approach is a new research area. Hence, the literature on such a hybrid cooling scheme are not abundant.
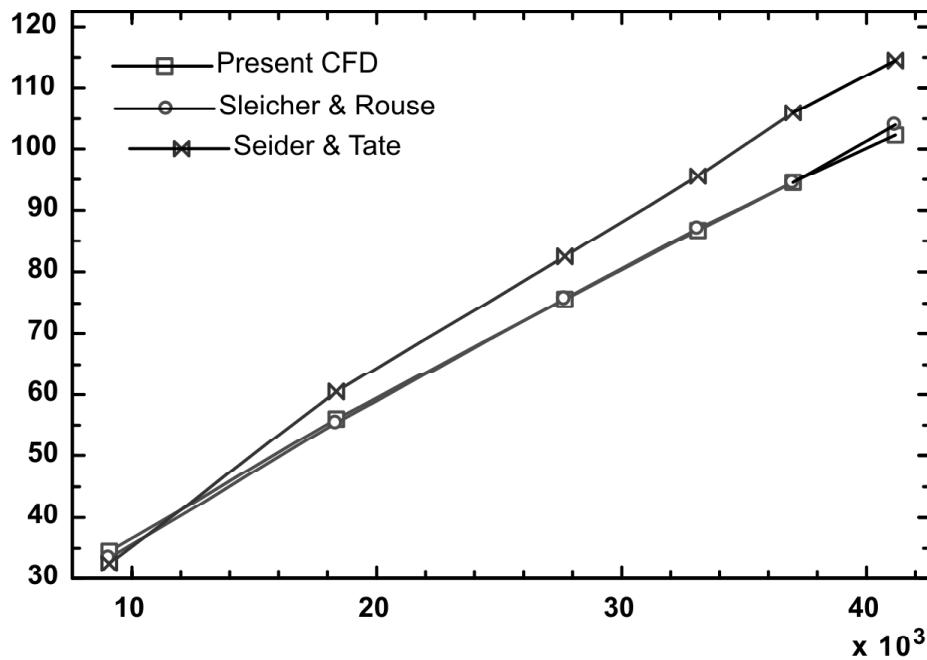

Figure 2: Validation curve for variation of average Nusselt number with duct Reynolds number

Nevertheless, the present numerical scheme is validated with Sleicher and Rouse [19] correlation by taking a three-dimensional circular pipe of diameter 0.026 m and length 0.67 m, and applying a uniform wall heat flux (i.e. 100 W/m^2) to the fully developed portion of the duct. This particular problem is chosen, since the boundary conditions for the validation purpose is similar to our present boundary conditions. A grid sensitivity test has also been carried out for the present validation, and it is found that a grid size of 28,891 cells predicted the surface Nusselt number reasonably well with the above correlation as shown in Fig. 2. However, the Sielder and Tate [20] correlation over predicts the Nusselt number since it is used for the fluids having a temperature dependent properties. As constant fluid properties are used in the present simulation, the computed values of Nusselt number are lower than the values reported in Ref. [21] and Ref. [23].

VI. RESULTS AND DISCUSSIONS

6.1. Grid independence test

A grid sensitivity test for the present numerical investigation from a ribbed surface with perforations in the presence of a cross flow jet is shown in Fig. 3. A few cells have been incorporated in the computational domain so as to start with the initial computation. The area weighted average Nusselt number gradually increases from 137 to 143.2 when the number cells in the doamin have been increased from 1,04,231 to 2,02,448 registering an increment of 4.89% in the Nusselt number. Thereafter, a small increase (0.003%) in the Nusselt number has been noticed when the number of cells is increased to 2,10, 380. Thus, The computational domain with 210, 380 cells is declared as the grid independence domain.
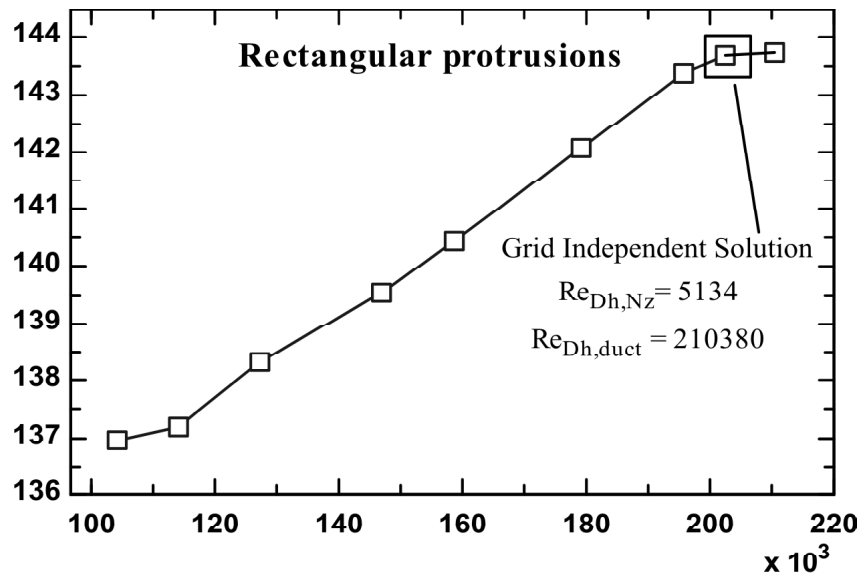

Figure 3: Variation of area weighted Nusselt number with the number of cells

6.2. Effect of duct Reynolds number on heat transfer rate

The effect of $Re_{Dh,Duct}$ on Nusselt number for two different (i.e., rectangular solid protrusion and rectangular protrusion with square perforations) have been illustrated in Fig. 4(a). For a particular nozzle Reynolds number ($Re_{Dh,Nz}$), the Nusselt number for both the cases has been increased monotonously with $Re_{Dh,Duct}$. It has been observed that the heat transfer enhancement with perforated protrusions is higher than that of the non-perforated (i.e., solid) protrusions. For example, the Nusselt number is improved by 16.1% when the solid protrusions are replaced by perforated protrusions at $Re_{Dh,Duct} = 46,000$.

As it could be seen from the velocity contours (see Fig. 4(b)-(c)) that the velocity of flow issuing out of the perforations is increased and causes a strong convection in the downstream side of the protrusions leading to a higher Nusselt number. In case of solid protrusions, although the flow recirculation reaches to the downstream side of the protrusions, the velocity of the circulatory flow is weakened because of the presence of the obstacle (i.e., the solid protrusion). The higher Nusselt number for perforated protrusions is evident from the temperature contour (Fig. 4(e)). As can be inferred from Fig. 4(d) and (e), a more uniform temperature near the heated surface has been noticed for the perforated protrusions than that of the solid protrusions.
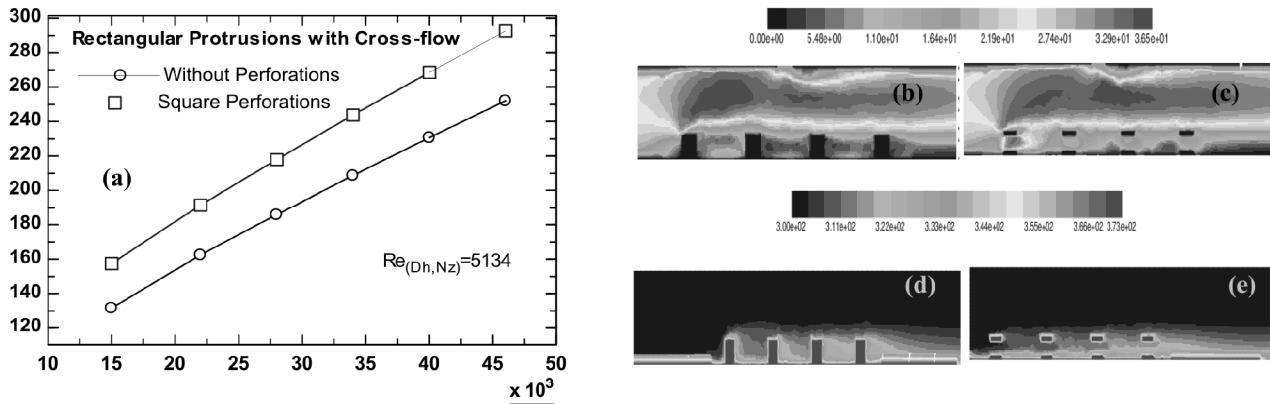
Figure 4: (a) Variation of area weighted average Nusselt number (Nu) with duct Reynolds number ($\mathrm{Re}_{Dh,Duct}$); velocity contours for (b) without perforations; (c) with square perforations; temperature contours for (d) without perforations; (e) with square perforations for $\mathrm{Re}_{Dh,Duct} = 40,000$

6.3. Comparison of heat transfer rate for the cross and without cross-flow effects

Comparative studies on the effects of the cross-flow and perforations have been studied. It has been seen that an increased heat transfer rate is obtained in a cross-flow case as compared to the non-cross-flow case. The heat transfer enhancement is independent of the solid or perforated protrusions. It is quite evident from Fig 5 (a) that heat transfer enhancement with perforated protrusions is quite higher that of the solid protrusions (see Fig. 5(a) black and blue colour line). Moreover, the deployment of a cross-flow jet enhances the heat transfer rate. For example, at $\mathrm{Re}_{Dh,Duct} = 15,000$, the Nusselt number has been improved by 11.27% when cross-flow arrangement is used for the perforated square protrusions (see blue and green lines from Fig. 5(a). Fig. 5(b) shows the velocity contours in $x - y$ plane passing through the mid-width of a duct fitted with rectangular protrusions with square perforations drilled in it. Fig. 5(c) shows the velocity contour for the same duct fitted with solid rectangular protrusions. As it could be seen (see Fig. 5(b)) that the velocity near the heated surface is higher when perforated protrusions are used. When the bottom wall fitted with solid protrusions, the velocity near the heated surface has been weakened, although a flow recirculation is observed in the inter-protrusion gaps.

The effect of the jet impingement on the characteristics of the mean flow has been seen from Fig. 5(a). The impinging jet presses the incoming fluid towards the heated surface; whereas the incoming fluid is diverted towards the top adiabatic wall when jet impingement is off (see Fig. 5(c)). Thus, the heat transfer with a jet impingement (i.e., with cross-flow effect) is found to be higher than the case without the jet impingement

6.4. Effect of duct Reynolds number on pressure drop and pumping power

In electronics cooling, to attain an efficient cooling strategy the pumping power as well as the pressure drops across the system needs to be reduced. Therefore, cooling strategies depend on the augmentation of the heat transfer rate, and the attenuation of the pressure drop and pumping power.

Fig. 6(a) shows the variation of pressure drop in duct Reynolds number. It could be seen that the pressure drop is increased with the duct Reynolds number. The pressure is the highest for a duct when the cross-flow and perforated protrusions are used. However, the increment of the pressure drop is not so high as compared to the other cases. A similar trend line has been seen for the pumping power variation with the duct Reynolds number shown in Fig. 6(b). Thus, it is important to study the effects of duct Reynolds numbers on the pumping power requirements. The pumping power is calculated as follows:
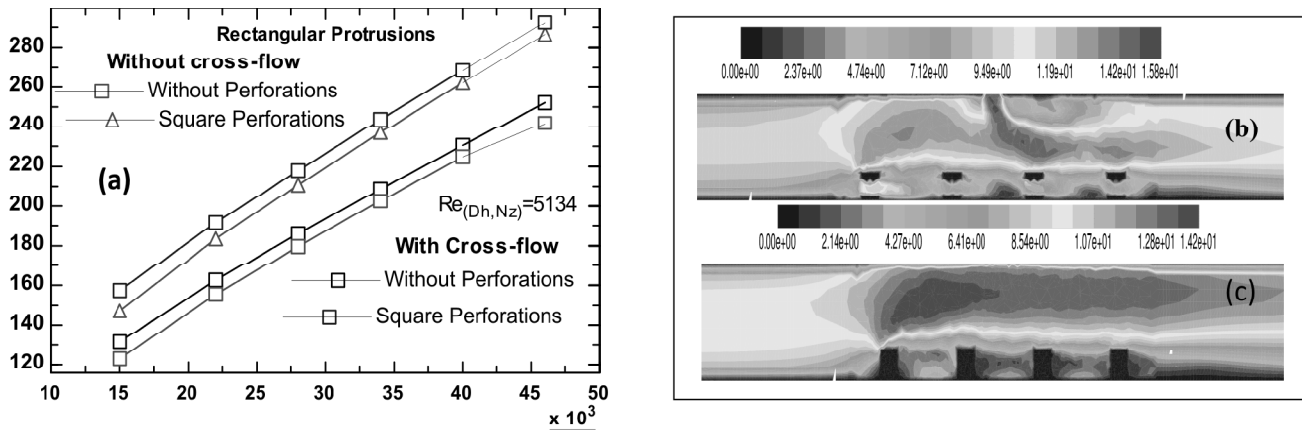
Figure 5: (a) Comparison of area weighted Nusselt number for cross-flow and without cross-flow (b) velocity contour for rectangular protrusion with square perforation and with cross-flow (c) velocity contour for rectangular protrusion without perforation and without cross-flow (expanded and cutaway)
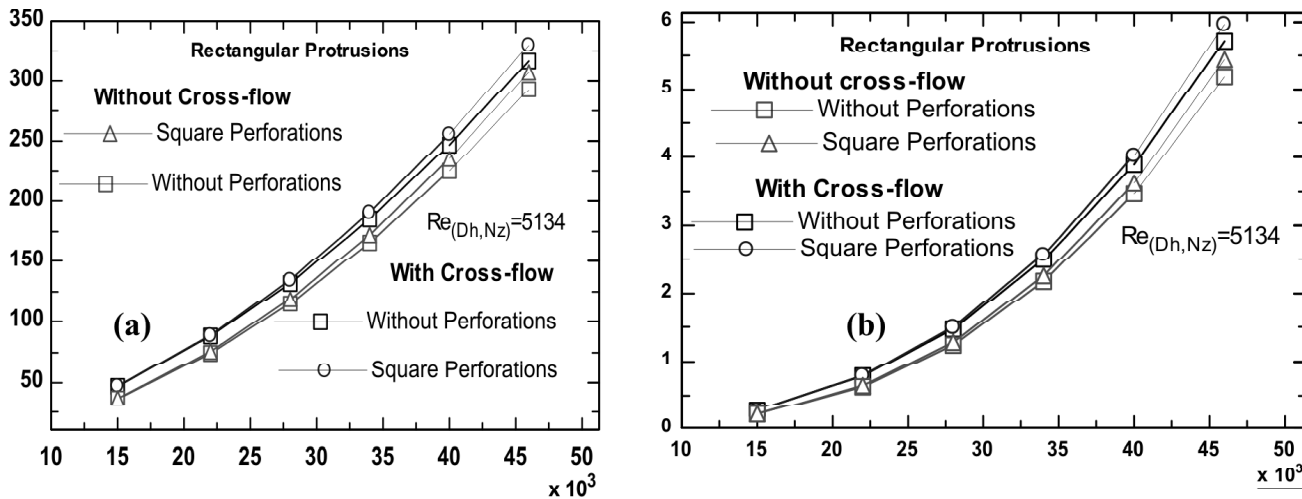

Figure 6: (a) Variation of pressure drop with duct Reynolds Number (b) Variation of Pumping Power with duct Reynolds number

Pumping power:

$$PP = \forall \times \Delta P \tag{14}$$

Where, $\forall$ total represents the total volume flow rate, which is the sum of the volume flow rates through inlets of the duct and nozzle. The pressure drop (ΔP) is calculated by taking the difference of inlets (nozzle and duct) and outlet pressures. For a particular value of $Re_{Dh,Nz}$, the pressure drop increases with the duct Reynolds number ($Re_{Dh,Duct}$) as has been depicted in Fig. 6(a). For lower duct Reynolds number, the increments in the pumping power and the pressure drop are rather low.

VII. CONCLUSION

The heat transfer enhancement in a rectangular duct with solid and perforated protrusions has been studied numerically employing the jet impingement. Following conclusions are drawn from the present study:

1.   A higher heat transfer rate has been observed when perforated surface protrusions are used instead of solid protrusions. At $Re_{Dh,Duct} = 46,000$, it has been observed that the Nusselt number is improved by

16.1 % as perforated protrusions are used instead of solid protrusions. This is because of a higher velocity of the incoming fluid in the vicinity of the heated wall.

2. Irrespective of the surface protrusions (perforated or solid), the heat transfer is found to be higher with the cross-flow jet arrangement than with the non-cross-flow arrangement. For instance, at $\text{Re}_{Dh,Duct} = 15,000$, the Nusselt number with cross-flow arrangement has been increased by 11.27% over the non-cross-flow arrangement.

3. A high pressure drop is obtained when both the cross-flow jet and protrusions with perforations are employed.

REFERENCES

[1] Mudawar,I. ,"Assessment of high-heat-flux thermal management schemes", in: Proceedings of the Seventh Intersociety *Conference on Thermal and Thermo mechanical Phenomena in Electronic Systems,* 1, 2000, pp. 1-20.

[2] Yeh,L. T., "Review of heat transfer technologies in electronic equipment", *ASME J. Electron. Packag.*117, 1995, pp.333–339.

[3] Prasad, B.N., and Saini, J.S.," Effect of artificial roughness on heat transfer and friction factor in a solar air heater", *Sol. Energy* 41, 1988, pp. 555-560.

[4] Gupta, D.,Solanki, S.C, and Saini,J.S.," Heat and fluid flow in rectangular solar air heater duct having transverse rib roughness on absorber plates", *Sol. Energy* 51, 1993, pp. 31-37.

[5] Lanjewar, A. Bhagoria, J.L., and Sarviya, R.M., "Heat transfer and friction in solar air heater duct with W-shaped rib roughness on absorber plate", *Energy* 36, 2011, pp. 4531-4541.

[6] Ebrahim Momin, A.M.,Saini, and Solanki, J. S., "Heat transfer and friction in solar air heater duct with V-shaped rib roughness on absorber plate", *Int. J. Heat Mass Transf.* 45, 2002, pp. 3383-3396.

[7] Karwa, R. B, and Karwa, K. N., "Experimental study of heat transfer enhancement in an asymmetrically heated rectangular duct with perforated baffles", *Int. Commun. Heat Mass Transf.* 32, 2005, pp. 275-284.

[8] Karwa, R. and Maheshwari, B.K., "Heat transfer and friction in an asymmetrically heated rectangular duct with half and fully perforated baffles at different pitches", *Int. Commun. Heat Mass Transf.* 36, 2009, pp. 264-268.

[9] Bhuiya, M.M.K., Chowdhury, M.S.U., Saha, and Islam ,M.T., "Heat transfer and friction factor characteristics in turbulent flow through a tube fitted with perforated twisted tape inserts", *Int. Commun. Heat Mass Transf.* 46, 2013,pp. 49-57.

[10] T. Alam, R.P. Saini, J.S. Saini, Experimental investigation on heat transfer enhancement due to V-shaped perforated blocks in a rectangular duct of solar air heater, Energy Convers. Manage. 81 (2014) 374e383.

[11] Zhou, G., Feng, Z. ,"Experimental investigations of heat transfer enhancement by stagnation region of an impinging plane jet"*, Int. J. Heat Mass Transf.* 40, 1997, pp. 3163-3176

[12] Zhou, G., Feng, Z., "Experimental investigations of heat transfer enhancement by stagnation region of an impinging plane jet"*, Int. J. Heat Mass Transf.* 40, 1997, pp. 3163-3176

[13] Didden, N., Didden, and Ho C.M., "Unsteady separation in a boundary layer produced by an impinging jet"*, J. Fluid Mech. 160* 1985,pp. 235-256.

[14] Gauntner,J., Livingoodn N.B, and Hrycak, P., "Survey of Literature on Flow Characteristics of a Single Turbulent Jet Impinging on a Flat Plate", *NASA, TN D*-5652,Lewis Research Centre, USA, 1970.

[15] A.K. Barik, S.Rout ,A. Mukherjee ,"Numerical investigation of heat transfer enhancement for a protruded surface by cross-flow jet using Al_2O_3-water nanofluid", *International journal Of heat And Mass transfer* 101,2016, pp. 550-561.

[16] Tan, L.,Zhang, J., andXu, H. "Jet impingement on a rib-roughened wall inside semi-confined channel", *Int. J. Therm. Sci.* 86, 2014, pp. 210-218.

[17] Su, L.M., and Chang,S.W., "Detailed heat transfer measurements of impinging jet arrays issued from grooved surfaces"*, Int. J. Therm. Sci.* 41, 2002, pp. 823-841.

[18]   A.K Barik, A. Mukherjee and P. Patro, "Heat transfer enhancement from a small rectangular channel with different surface protrusions by a turbulent cross flow jet". *Int. Journal of Thermal Science*. 98, 2015, pp. 32-41.

[19]   Zuckerman, N. and Lior, N., "Impingement heat transfer: correlations and numerical modelling", *ASME J. Heat Transfer*, 127, 2005, pp. 544-552.

[20]   C.A. Slicher, M.W. Rouse, A convenient correlation for heat transfer to constant and variable property fluids in turbulent pipe flow, *International. Journal. Heat Mass Transfer.* 18 (1975) 677e683.

[21]   E.N. Sieder, G.E. Tate, Heat transfer and pressure drop of liquids in tubes, Ind. Eng. Chem. 28 (1936) 1429e1436.

[22]   F.R. Menter, Two-equation eddy-viscosity turbulence models for engineering applications, AIAA J. 32 (1994) 1598e1605

[23]   A. K. Barik, S. K. Dash, A. Guha, Experimental and numerical investigation of air entrainment into an infrared suppression device*, Appl. Therm. Eng*. 75 (2015) 33–44.